Proceedings of the ASME 2008 International Design Engineering Technical Conferences & Computers and Information in Engineering Conference
IDETC/CIE 2008
August 3-6, 2008, Brooklyn, New York, USA

DETC2008-49931

DEVELOPMENT OF A SELF-EXCITED OSCILLATOR FOR SI-TRACEABLE MEASUREMENTS IN ATOMIC FORCE MICROSCOPY

Gregory W. Vogl*
Jon R. Pratt
Manufacturing Engineering Laboratory
National Institute of Standards and Technology
Gaithersburg, Maryland 20899-8221
Email: gvogl@nist.gov

ABSTRACT

A new self-excited micro-oscillator is proposed as a velocity reference that could aid the dissemination of nanonewton-level forces that are traceable to the International System of Units (SI). An analog control system is developed to keep the actuation side of the device oscillating sinusoidally with an amplitude that is fairly insensitive to the quality factor. Consequently, the device can be calibrated as a velocity reference in air and used in ultra-high vacuum with a velocity shift of less than one percent. Hence, the calibrated micro-oscillator could be used with electrostatic forces to calibrate cantilevers used for atomic force microscopy (AFM) as SI-traceable force transducers. Furthermore, the calibrated micro-oscillator could potentially be used as an AFM sensor to achieve atomic resolutions on par with those realized in frequency-modulation AFM (FM-AFM) with quartz tuning forks.

INTRODUCTION

Since the development of AFM [1], the method has been used to achieve atomic resolution [2, 3] and to characterize electrical, magnetic, and mechanical properties of materials. However, commercial AFM suffers from a lack of accurate force measurements because there is presently no method to disseminate SI-traceable nanonewton-level forces to most AFM users. This situation concerns AFM users who need to measure and control the small forces between an AFM cantilever tip and the substrate surface, e.g., in single-molecule force spectroscopy [4, 5]. Traceability is also needed to compare AFM force measurements to those made by optical tweezers and other methods.

Currently, calibration has focused on methods to determine the cantilever stiffness. Accordingly, tip-sample forces are usually calculated by Hooke's law ($F = kx$) with an estimated cantilever stiffness (k) and a measured tip deflection (x). For example, dynamic methods for estimation of the stiffness usually rely on the thermal noise spectrum [6, 7], the resonant frequency shift with added mass [8], or the resonant frequency with knowledge of the cantilever density and dimensions [9]. While possibly being efficient or available for *in situ* AFM cantilever calibration, these methods do not yield SI-traceable cantilever stiffnesses because of the lack of SI-traceable forces. Alternatively, traceable forces from calibrated masses [10] or reference cantilevers calibrated with an electrostatic force balance [11] may be used for static cantilever calibrations, but these methods are usually not efficient or available for *in situ* AFM cantilever calibration, particularly in extreme cryogenic environments.

PROPOSED DEVICE

A new self-excited oscillator is proposed to allow SI-traceable calibrations of AFM cantilevers in several environments [12]. The proposed micro-oscillator is composed of a sensing side and an actuation side, as outlined in Fig. 1(a). The actuation side is attached to a rigid substrate (not shown) through two flexures, while the sensing side is attached to the actuation side by a thin flexure. Magnetic sensing and actuation are possible because both sides of the device are top-coated with magnetic thin films and closely surrounded by conductive microwires. Accordingly, the rotational velocity of the sensing side is observed

*Address all correspondence to this author.

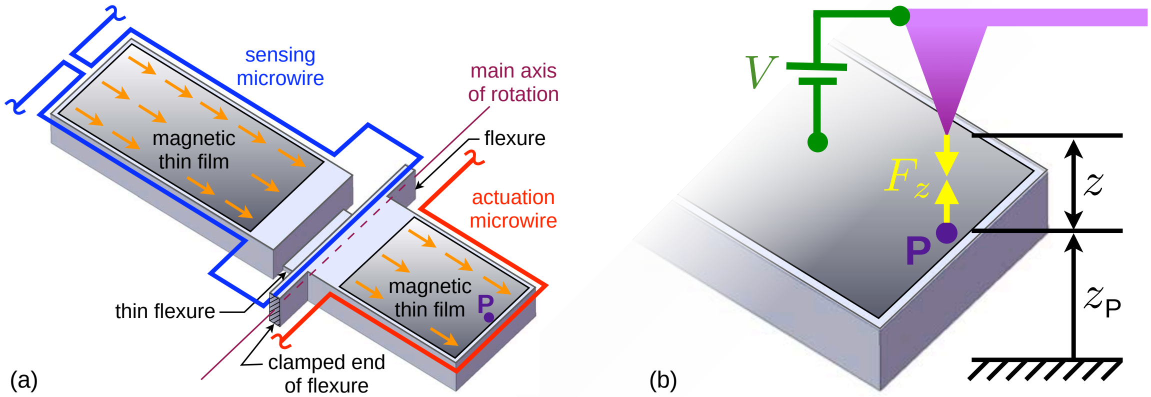

Figure 1. (a) PROPOSED MICRO-OSCILLATOR THAT IS COMPOSED OF A SENSING-SIDE (LEFT) AND AN ACTUATOR SIDE (RIGHT) THAT ARE TOP-COATED IN MAGNETIC THIN FILMS, WHICH ARE MAGNETIZED LENGTHWISE AND CLOSELY SURROUNDED BY MICROWIRES, AND (b) A SCHEMATIC OF THE ACTUATION SIDE OF THE DEVICE DURING AN AFM CANTILEVER CALIBRATION. THE DEVICE IS NOT TO SCALE.

in the sensing current according to Faraday's law of magnetic induction, while the interaction of the actuation current with the magnetic thin film produces a torque on the actuation side.

The device modeling and control will be described in this paper. However, the potential use of the micro-oscillator for traceable AFM cantilever calibrations is explained first.

DEVICE AS VELOCITY STANDARD

During calibration of an AFM cantilever, the small forces applied to the cantilever will be non-contact and electrostatic in nature. As seen in Fig. 1(b), the cantilever tip is brought very close above point P, with a vertical separation z between the tip and the device. A known voltage V is then applied across the "capacitor", which is the cantilever-device system with capacitance C. Consequently, a net vertical electrostatic force exists with a magnitude F_z that is defined by

$$F_z = \frac{1}{2}\left|\frac{dC}{dz}\right|V^2 \tag{1}$$

Hence, once the capacitance gradient dC/dz is determined, the electrostatic force F_z will be known. In fact, the vibration at point P will be calibrated and used to determine dC/dz.

Understanding how the velocity of point P is used to determine the capacitance gradient begins by noting that the charge q and the potential difference V for a capacitor are proportional to each other through the capacitance; that is,

$$q = CV \tag{2}$$

Hence, the displacement current $i = dq/dt$ is

$$i = \frac{d}{dt}(CV) \tag{3}$$

Because the capacitance C changes only with the gap distance z, the current becomes

$$i = \frac{dC}{dz}\frac{dz}{dt}V_0 \tag{4}$$

when the gap distance varies with time t while the voltage remains constant at V_0.

Next, we assume that the vibration frequency of the device is far away from all resonant frequencies of the AFM cantilever. Consequently, the cantilever will not be excited and can be regarded as fixed during the device oscillation, which means that

$$\frac{dz}{dt} = -\frac{dz_{\mathrm{P}}}{dt} \tag{5}$$

by inspection of Fig. 1(b). Furthermore, if point P oscillates with a sufficiently small amplitude such that the capacitance gradient is essentially constant over the oscillation range, then the root mean square (rms) of the current becomes

$$i_{\mathrm{rms}} = \left|\frac{dC}{dz}\right||V_0|\left(\frac{dz_{\mathrm{P}}}{dt}\right)_{\mathrm{rms}} \tag{6}$$

according to Eqn. (4). Finally, we solve for the capacitance gradient and substitute the result into Eqn. (1) to obtain

$$F_z = \frac{i_{\mathrm{rms}}|V_0|}{2\left(\dot{z}_{\mathrm{P}}\right)_{\mathrm{rms}}} \tag{7}$$

where the overdot represents differentiation with respect to time.

Equation (7) reveals that if traceable measurements of voltage V_0, rms current i_{rms}, and velocity of point P are obtained during calibration of an AFM cantilever, then the electrostatic force F_z is known with SI-traceability. Moreover, if the velocity of point P is the same before and during AFM cantilever calibrations, then the microdevice can be calibrated as a velocity standard for subsequent cantilever calibrations. The enabling of velocity calibration *ex situ* would be an alternative to the *in situ* velocity calibration performed by Cumpson and Hedley [13] for the application of traceable electrostatic forces with a micro-oscillator.

APPROXIMATE MODEL

Before controlling the device for use as a velocity standard, the system is modeled as a two-degree-of-freedom system. The sensing and actuation masses are treated as rigid bodies that rotate with angles ψ and θ about one fixed central axis, as seen in Fig. 2. The rotational inertias of the sensing and actuation sides about the central axis are I_s and I_a, respectively. The torsional stiffness of the actuation side is κ_a, while the torsional stiffness of the sensing side is κ_s relative to the actuation side. Consequently, the fundamental frequencies used for the simplified model are ω_s and ω_a and are defined by $\omega_\mathrm{s}^2 = \kappa_\mathrm{s}/I_\mathrm{s}$ and $\omega_\mathrm{a}^2 = \kappa_\mathrm{a}/I_\mathrm{a}$, respectively.

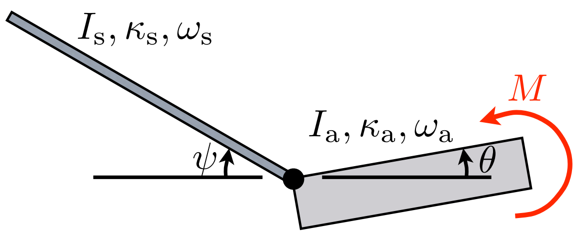

Figure 2. APPROXIMATE MODEL OF PROPOSED MICRO-OSCILLATOR.

For a net applied moment M on the actuation side, as seen in Fig. 2, the rotational form of Newton's second law yields the two equations of motion,

$$I_\mathrm{s}\ddot{\psi} + 2\zeta_\mathrm{s} I_\mathrm{s}\omega_\mathrm{s}\dot{\psi} + \kappa_\mathrm{s}(\theta+\psi) = 0 \tag{8a}$$

$$I_\mathrm{a}\ddot{\theta} + 2\zeta_\mathrm{a} I_\mathrm{a}\omega_\mathrm{a}\dot{\theta} + \kappa_\mathrm{s}(\theta+\psi) + \kappa_\mathrm{a}\theta = M \tag{8b}$$

where linear damping has been assumed to exist with the viscous damping factors ζ_s and ζ_a for the sensing and actuation sides, respectively.

We nondimensionalize time as $\bar{t} = \omega_\mathrm{s} t$ and subsequently nondimensionalize Eqns. (8) to obtain

$$\psi'' + 2\zeta_\mathrm{s}\psi' + \psi + \theta = 0 \tag{9a}$$

$$\lambda\theta'' + 2\zeta_\mathrm{a}\lambda\beta\theta' + (1+\lambda\beta^2)\theta + \psi = \tau \tag{9b}$$

where the prime represents differentiation with respect to the nondimensional time $\bar{t}$, $\lambda = I_\mathrm{a}/I_\mathrm{s}$, $\beta = \omega_\mathrm{a}/\omega_\mathrm{s}$, and $\tau = M/\kappa_\mathrm{s}$. We note that $\lambda\beta^2 = \kappa_\mathrm{a}/\kappa_\mathrm{s}$ and represents the relative torsional stiffnesses of the oscillator sides. Equations 9 are used for the system analysis and control described herein.

DESIGN GOALS

The system parameters (λ and β) and forcing function (τ) for Eqns. (9) must be chosen to achieve three goals regarding the system oscillation:

1. The sensing angle ψ is generally much larger than the actuation angle θ.
2. The actuation angle θ approaches a sinusoidal limit cycle.
3. The sinusoidal limit cycle for θ is fairly insensitive to the quality factor $Q = 1/2\zeta_\mathrm{s}$.

Goal 1 will give us a "mechanical advantage" to boost the sensing current and consequently decrease the gain required to create the actuation current.

Goal 2 will ensure a precise sinusoidal motion that is desired for calibration purposes. Firstly, we could measure the rms signal and simply determine its amplitude if needed. Secondly, the device should operate with only one frequency component to minimize the chances of exciting an AFM cantilever during calibration.

Goal 3 ensures a reliable motion despite possible changes in Q. Therefore, the oscillator could be calibrated as a velocity standard *ex situ* (like in air) and then used with a minor shift in velocity for AFM cantilever calibrations *in situ* (like in vacuum).

TWO PHYSICAL RANGES THAT ACHIEVE GOAL 1

Goal 1 means that the order of the sensing motion is much greater than the order of the actuation motion; that is, $\mathrm{O}(\psi) \gg \mathrm{O}(\theta)$. This goal can be achieved by having the sensing side resonate in a high-Q environment while the actuation side is far away from resonance. Hence, the fundamental frequency of the actuation side should be much larger ($\beta \gg 1$) or smaller ($\beta \ll 1$) than the resonant frequency of the sensing side.

Two cases achieve Goal 1. For the "stiff" case ($\beta \gg 1$ and $\lambda\beta^2 \gg 1$), the actuation side has a much larger fundamental frequency than the sensing side ($\omega_\mathrm{a} \gg \omega_\mathrm{s}$) and the actuation side is rotationally much stiffer than the sensing side ($\kappa_\mathrm{a} \gg \kappa_\mathrm{s}$). Equation 9b becomes approximately

$$\lambda\beta^2\theta + \psi = \tau \tag{10}$$

On the other hand, for the "heavy" case ($\beta \ll 1$ and $\lambda \gg 1$), the actuation side has a much smaller fundamental frequency than the sensing side ($\omega_\mathrm{a} \ll \omega_\mathrm{s}$) and the actuation side is rotationally much heavier than the sensing side ($I_\mathrm{a} \gg I_\mathrm{s}$). Equation 9b becomes approximately

$$\lambda\theta'' + \psi = \tau \tag{11}$$

For relatively small forcing τ, Eqns. (10) and (11) show that $\mathrm{O}(\psi) \gg \mathrm{O}(\theta)$, as desired to achieve Goal 1, because $\lambda\beta^2 \gg 1$ or $\lambda \gg 1$, respectively.

INITIAL ATTEMPT AT FORCING FUNCTION TO ACHIEVE GOAL 2

Since the ranges of the system parameters (λ and β) were determined by achieving Goal 1, the forcing function (τ) will be determined by achieving Goals 2 and 3.

To satisfy Goal 2, we need to choose τ so that the actuation angle θ approaches a sinusoidal limit cycle. The nondimensional torque τ is at our disposal but must be a function of the sensed angular velocity ψ', just as the dimensional torque M is at our disposal but must be a function of the sensed current. Consequently, one approach is to let

$$\tau = -\epsilon\left[\psi' - \alpha(\psi')^3\right] \tag{12}$$

where ϵ and α are constants. The Rayleigh forcing [14] in Eqn. (12) is one of the simplest velocity-dependent forcings that can yield limit cycles in single-degree-of-freedom systems.

Stiffness-Dominated Case

For the "stiff" case, we substitute Eqn. (12) into Eqn. (10) to find out that

$$\theta = -\frac{1}{\lambda\beta^2}\left\{\psi + \epsilon\left[\psi' - \alpha(\psi')^3\right]\right\} \tag{13}$$

which is then substituted into Eqn. (9a) to yield

$$\psi'' + \left(2\zeta_{\mathrm{s}} - \frac{\epsilon}{\lambda\beta^2}\right)\psi' + \psi = -\frac{\epsilon\alpha}{\lambda\beta^2}(\psi')^3 \tag{14}$$

which is like a Rayleigh equation [14]. Because the second goal is for θ to approach a sinusoidal limit cycle, we see by inspection of Eqn. (13) that ψ should also approach a sinusoidal limit cycle and that ϵ should somehow be "small."

For the sensing angle ψ to approach a limit cycle, the linear system of Eqn. (14) must be unstable, which means that $2\zeta_{\mathrm{s}} < \epsilon/\lambda\beta^2$ by inspection. We want the system to be far from its stability boundary, so we let

$$2\zeta_{\mathrm{s}} \ll \frac{\epsilon}{\lambda\beta^2} \tag{15}$$

which yields approximately

$$\psi'' + \psi = \frac{\epsilon}{\lambda\beta^2}\left[\psi' - \alpha(\psi')^3\right] \tag{16}$$

However, in order for the solution of Eqn. (16) to be sinusoidal, we must have that (cf. Ref. [14])

$$\frac{\epsilon}{\lambda\beta^2} \ll 1 \tag{17}$$

which yields

$$\psi \approx \sqrt{\frac{4}{3\alpha}}\cos(\bar{t} + \varphi) \tag{18}$$

where φ is a phase that depends upon initial conditions. When Eqn. (18) is substituted into Eqn. (13), we find out that

$$\epsilon \ll 3 \tag{19}$$

in order for $\theta \approx -\psi/\lambda\beta^2$ and hence approximately sinusoidal. We note that Eqn. (17) is satisfied when Eqn. (19) is satisfied because $\lambda\beta^2 \gg 1$.

Therefore, in order for θ to approach an approximately sinusoidal limit cycle with the Rayleigh forcing in Eqn. (12), we must have that

$$\frac{\lambda\beta^2}{Q} \ll \epsilon \ll 3 \tag{20}$$

according to Eqns. (15) and (19) with $Q = 1/2\zeta_{\mathrm{s}}$. In other words, the nondimensional forcing magnitude ϵ must not be too small or too large but "just right" in order for Goal 2 to be achieved for the "stiff" case ($\beta \gg 1$ and $\lambda\beta^2 \gg 1$).

Because $|\psi/\theta| \approx \lambda\beta^2$, it is desirable to have $\lambda\beta^2 \geq 100$ for the largest "mechanical advantage." However, we could then need $1 \ll \epsilon \ll 3$ in air when $Q = 100$, according to Eqn. (20), which is not possible. Hence, θ cannot approach a fairly sinusoidal limit cycle for the "stiff" case with the given Rayleigh forcing.

Inertia-Dominated Case

Perhaps a sinusoidal limit cycle can be achieved for the "heavy" case. We substitute Eqn. (12) into Eqn. (11) to find out that

$$\theta'' = -\frac{1}{\lambda}\left\{\psi + \epsilon\left[\psi' - \alpha(\psi')^3\right]\right\} \tag{21}$$

If sinusoidal motion exists, $\theta'' \approx -\theta$ because $\mathrm{O}(d/d\bar{t}) \approx 1$, so Eqn. (21) becomes

$$\theta = \frac{1}{\lambda}\left\{\psi + \epsilon\left[\psi' - \alpha(\psi')^3\right]\right\} \tag{22}$$

Next, by following the same procedure as for the "stiff" case, we find out that $\epsilon < 0$ and

$$\frac{\lambda}{Q} \ll |\epsilon| \ll 3 \tag{23}$$

in order for θ to approach an approximately sinusoidal limit cycle. For this "heavy" case, because $|\psi/\theta| \approx \lambda$, it is desirable to have $\lambda \geq 100$ for the largest "mechanical advantage." However, like for the "stiff" case, we would then need $1 \ll |\epsilon| \ll 3$ when $Q = 100$, according to Eqn. (23), which is not possible.

SYSTEM THAT ACHIEVES GOALS 1 AND 2

Thus far, we have shown that a sinusoidal limit cycle for θ is not possible in air for the system

$$\psi'' + 2\zeta_\mathrm{s}\psi' + \psi + \theta = 0 \tag{24a}$$

$$\lambda\theta'' + 2\zeta_\mathrm{a}\lambda\beta\theta' + (1+\lambda\beta^2)\theta + \psi = -\epsilon\left[\psi' - \alpha(\psi')^3\right] \tag{24b}$$

Consequently, the Rayleigh forcing in Eqn. (24b) needs to be changed in order to achieve Goal 2.

We start by rearranging the system as

$$\psi'' + 2\zeta_\mathrm{s}\psi' + \psi + \theta = 0 \tag{25a}$$

$$\lambda\theta'' + 2\zeta_\mathrm{a}\lambda\beta\theta' + (1+\lambda\beta^2)\theta + \psi = -\epsilon\left[1 - \alpha(\psi')^2\right]\psi' \tag{25b}$$

Then we note that to obtain sinusoidal limit cycles, the system forcing must also be sinusoidal. This means that $(\psi')^2$ in Eqn. (25b) must be filtered so that the 2nd-harmonic term is significantly reduced. Accordingly, we filter $(\psi')^2$ with a second-order Butterworth filter to obtain the system

$$\psi'' + 2\zeta_\mathrm{s}\psi' + \psi + \theta = 0 \tag{26a}$$

$$\lambda\theta'' + 2\zeta_\mathrm{a}\lambda\beta\theta' + (1+\lambda\beta^2)\theta + \psi = -\epsilon\left[1 - \alpha\Psi\right]\psi' \tag{26b}$$

$$\Psi'' + 2\zeta_\mathrm{f}\omega_\mathrm{f}\Psi' + \omega_\mathrm{f}^2\Psi = \omega_\mathrm{f}^2(\psi')^2 \tag{26c}$$

where Ψ is the filtered version of $(\psi')^2$, ω_f is the cutoff frequency of the filter, and ζ_f is the viscous damping factor of the filter. A second-order Butterworth filter was chosen because it rolls off faster than a first-order Butterworth filter and is still easily implemented in an analog circuit.

By letting $\omega_\mathrm{f} \lll 2$, the DC term of $(\psi')^2$ is kept but the 2nd-harmonic term is filtered out, as desired. If ψ is sinusoidal, the forcing on the right-hand side of Eqn. (26b) is then sinusoidal. Accordingly, the system described by Eqns. (26) is able to have sinusoidal limit cycles.

For example, limits cycles for the unfiltered system (Eqns. (24)) and the filtered system (Eqns. (26)) with the same parameters are shown in Fig. 3. The limit cycles in Fig. 3(a) exhibit significant 3rd-harmonics, especially the limit cycle for θ, which we desire to be sinusoidal. This non-sinusoidal behavior was expected for the unfiltered system, because the parameter ϵ does not satisfy Eqn. (20) for this "stiff" case. Also, Goal 1 is not achieved because the amplitudes are on the same order. On the other hand, the limit cycles in Fig. 3(b) are sufficiently sinusoidal because of the filter in Eqn. (26c). Furthermore, Goal 1 is satisfied because ψ is generally much larger than θ. We also note that it does not matter that θ lags behind ψ, because only the motion of θ will be measured for a velocity standard.

LIMIT CYCLES FOR FILTERED SYSTEM

As seen in Fig. 3(b), the filtered system in Eqns. (26) yields limit cycles that are sinusoidal (Goal 2); that is,

$$\psi \to A_\psi \cos(\bar{\omega}\bar{t} + \varphi_\psi) \tag{27a}$$

$$\theta \to A_\theta \cos(\bar{\omega}\bar{t} + \varphi_\theta) \tag{27b}$$

as $\bar{t} \to \infty$, in which A_ψ and A_θ are the amplitudes, φ_ψ and φ_θ are the phases that depend on the initial conditions, and $\bar{\omega}$ is the nondimensional limit cycle frequency. Also, the amplitude A_ψ of sensing motion is much larger than the amplitude A_θ of actuation motion (Goal 1).

However, the amplitude A_θ depends significantly on the quality factor Q. For example, Fig. 4 shows how ψ has a fairly constant amplitude while the amplitude of θ varies with Q. The same behavior exists for the "heavy" case, as well. Thus, Goal 3 is not yet satisfied, so the system must be changed somehow to achieve this goal. However, the system response must be better understood before it can be controlled.

"Stiff" Limit Cycles

The sinusoidal limit cycles for the "stiff" filtered system can be easily obtained. First, for a nearly perfect filter,

$$\Psi \to \frac{(\bar{\omega}A_\psi)^2}{2} \tag{28}$$

as $\bar{t} \to \infty$ because Ψ will approach the DC component of $(\psi')^2$. Therefore, for the "stiff" system with $\beta \gg 1$ and $\lambda\beta^2 \gg 1$, Eqn. (26b) will limit to approximately

$$\lambda\beta^2\theta + \psi = -\epsilon\left[1 - \alpha\frac{(\bar{\omega}A_\psi)^2}{2}\right]\psi' \tag{29}$$

which means that

$$\theta \to -\frac{1}{\lambda\beta^2}\left\{\psi + \epsilon\left[1 - \alpha\frac{(\bar{\omega}A_\psi)^2}{2}\right]\psi'\right\} \tag{30}$$

as $\bar{t} \to \infty$.

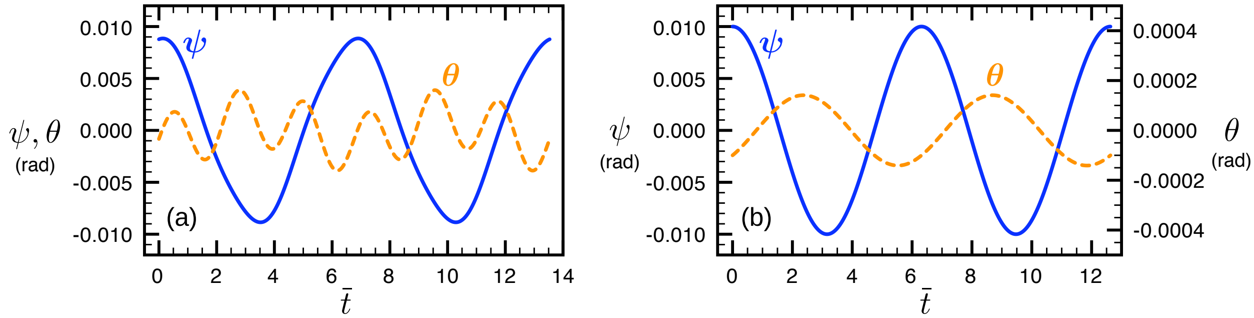

Figure 3. EXAMPLES OF LIMIT CYCLES FOR (a) THE UNFILTERED SYSTEM GIVEN IN EQNS. (24) AND (b) THE FILTERED SYSTEM DEFINED BY EQNS. (26). PARAMETERS USED FOR BOTH SUBFIGURES ARE $\beta = 10$, $\lambda = 1$, $\zeta_\mathrm{s} = \zeta_\mathrm{a} = 0.005$, $\epsilon = 100$, AND $\alpha = 20000$. THE PARAMETERS $\omega_\mathrm{f} = 0.00001$ AND $\zeta_\mathrm{f} = 1$ WERE ALSO USED FOR THE FILTERED SYSTEM.

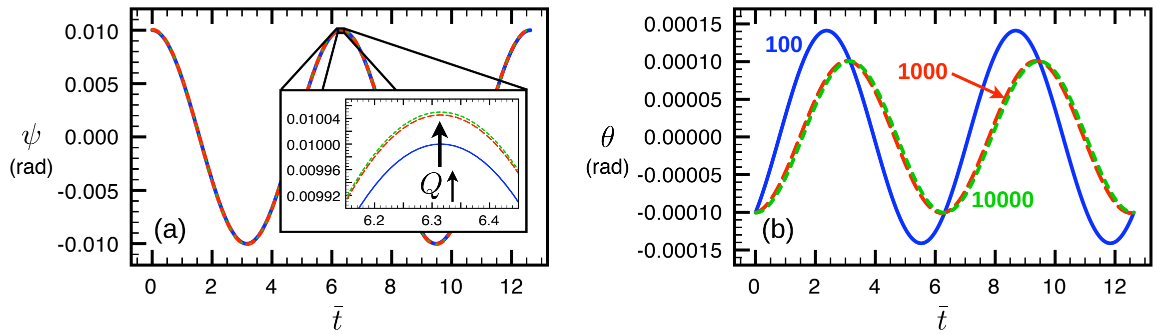

Figure 4. LIMIT CYCLES FOR (a) ψ AND (b) θ FOR THE FILTERED SYSTEM (EQNS. (26)) WITH $Q = 100$, 1000, OR 10000. THE OTHER PARAMETERS USED ARE $\beta = 10$, $\lambda = 1$, $\zeta_\mathrm{a} = \zeta_\mathrm{s}$, $\epsilon = 100$, $\alpha = 20000$, $\omega_\mathrm{f} = 0.00001$, AND $\zeta_\mathrm{f} = 1$.

Next, substitution of Eqn. (30) into Eqn. (26a) yields

$$\psi'' + \left\{2\zeta_\mathrm{s} - \frac{\epsilon}{\lambda\beta^2}\left[1 - \alpha\frac{(\bar{\omega}A_\psi)^2}{2}\right]\right\}\psi' + \left(1 - \frac{1}{\lambda\beta^2}\right)\psi = 0 \tag{31}$$

for the limit cycle. Furthermore, the damping in Eqn. (31) must equal zero because the limit cycle exists; that is,

$$\epsilon\left[1 - \alpha\frac{(\bar{\omega}A_\psi)^2}{2}\right] = \frac{\lambda\beta^2}{Q} \tag{32}$$

The remaining undamped system reveals that

$$\bar{\omega}^2 = 1 - \frac{1}{\lambda\beta^2} \tag{33}$$

Hence, because $\bar{\omega} \approx 1$ for $\lambda\beta^2 \gg 1$, Eqn. (32) shows that

$$A_\psi^2 \approx \frac{2}{\alpha}\left(1 - \frac{\lambda\beta^2}{\epsilon Q}\right) \tag{34}$$

Equation 34 reveals that $A_\psi \approx \sqrt{2/\alpha}$ when ϵ is sufficiently large. Indeed, Fig. 4(a) shows that $A_\psi \approx 0.01 = \sqrt{2/\alpha} = \sqrt{2/20000}$ even as Q varies. In fact, the amplitude A_ψ will increase slightly as Q increases, according to Eqn. (34). This subtle behavior is seen in the insert of Fig. 4(a).

Yet, the limit cycle amplitude A_θ varies significantly with Q, as known from Fig. 4(b). Substitution of Eqn. (32) into Eqn. (30) yields

$$\theta \to -\frac{1}{\lambda\beta^2}\left\{\psi + \frac{\lambda\beta^2}{Q}\psi'\right\} \tag{35}$$

as $\bar{t} \to \infty$, which means that

$$A_\theta \approx A_\psi\sqrt{\left(\frac{1}{\lambda\beta^2}\right)^2 + \left(\frac{1}{Q}\right)^2} \tag{36}$$

according to Eqns. (27). Now that the actuation amplitude A_θ is known analytically, a control scheme can be devised to achieve Goal 3 for the "stiff" case.

“Heavy” Limit Cycles

By following a similar procedure as that for the “stiff” case, we find out that

$$\epsilon\left[1-\alpha\Psi\right] = -\frac{\lambda}{Q} \tag{37}$$

and

$$\bar{\omega}^2 = 1+\frac{1}{\lambda} \tag{38}$$

for the “heavy” limit cycle response ($\beta \ll 1$ and $\lambda \gg 1$). Consequently, we determine that

$$A_\psi^2 \approx \frac{2}{\alpha}\left(1+\frac{\lambda}{\epsilon Q}\right) \tag{39}$$

and

$$\theta \to \frac{1}{\lambda}\left\{\psi - \frac{\lambda}{Q}\psi'\right\} \tag{40}$$

as $\bar{t}\to\infty$, so that

$$A_\theta \approx A_\psi\sqrt{\frac{1}{\lambda^2}+\frac{1}{Q^2}} \tag{41}$$

DAMPING-DEPENDENT GAIN FOR AMPLITUDE CONTROL (GOAL 3)

Thus far, we have determined that sinusoidal limit cycles (Goal 2) are achieved and that $A_\psi \gg A_\theta$ (Goal 1) for the filtered system described in Eqns. (26). Also, we derived analytical approximations for the limit cycles. The limit cycles were found to have amplitudes A_ψ and A_θ of

$$A_\psi \approx \begin{cases}\sqrt{\frac{2}{\alpha}\left(1-\frac{\lambda\beta^2}{\epsilon Q}\right)}, & \text{“stiff” case}\\ \sqrt{\frac{2}{\alpha}\left(1+\frac{\lambda}{\epsilon Q}\right)}, & \text{“heavy” case}\end{cases} \tag{42a}$$

$$A_\theta \approx \begin{cases}A_\psi\sqrt{\left(\frac{1}{\lambda\beta^2}\right)^2+\left(\frac{1}{Q}\right)^2}, & \text{“stiff” case}\\ A_\psi\sqrt{\frac{1}{\lambda^2}+\frac{1}{Q^2}}, & \text{“heavy” case}\end{cases} \tag{42b}$$

with a limit cycle nondimensional frequency $\bar{\omega}$ of

$$\bar{\omega} \approx \begin{cases}\sqrt{1-\frac{1}{\lambda\beta^2}}, & \text{“stiff” case}\\ \sqrt{1+\frac{1}{\lambda}}, & \text{“heavy” case}\end{cases} \tag{43}$$

and a nondimensional adaptive feedback gain of

$$\epsilon\left[1-\alpha\Psi\right] \approx \begin{cases}\frac{\lambda\beta^2}{Q}, & \text{“stiff” case}\\ -\frac{\lambda}{Q} & \text{“heavy” case}\end{cases} \tag{44}$$

Now, we postulate that we can let the gain ϵ vary with the quality factor Q such that $A_\theta \not\approx f(Q)$ (Goal 3). Indeed, we find out that when

$$\epsilon \approx \begin{cases}\frac{Q}{\lambda\beta^2}+\frac{\lambda\beta^2}{Q}, & \text{“stiff” case}\\ -\left(\frac{Q}{\lambda}+\frac{\lambda}{Q}\right) & \text{“heavy” case}\end{cases} \tag{45}$$

the amplitude A_θ is approximately

$$A_\theta \approx \begin{cases}\frac{1}{\lambda\beta^2}\sqrt{\frac{2}{\alpha}} & \text{“stiff” case}\\ \frac{1}{\lambda}\sqrt{\frac{2}{\alpha}}, & \text{“heavy” case}\end{cases} \tag{46}$$

which is independent of Q, as desired.

Therefore, the third goal of having $A_\theta \not\approx f(Q)$ is achieved when ϵ satisfies Eqn. (45). For example, Fig. 5(b) shows how θ has a sinusoidal limit cycle with an amplitude that varies little with Q, in contrast with the responses in Fig. 4(b).

FINAL SYSTEM THAT ACHIEVES ALL GOALS

The nondimensional gain ϵ in Eqn. (45) depends on the quality factor Q, which may neither be known *a priori* nor measured during operation. So, ϵ needs to vary with Q without its value being explicitly known. We achieve this goal by using a known signal that depends on Q in a predictable way. Specifically, substitution of Eqn. (44) into Eqn. (45) reveals that

$$\epsilon \approx \epsilon\left[1-\alpha\Psi\right] + \frac{1}{\epsilon\left[1-\alpha\Psi\right]} \tag{47}$$

for either the “stiff” or “heavy” limit cycle. Equation 47 shows that the optimal gain ϵ depends on itself through the “adaptive feedback gain.”

In order for ϵ to approach the desired value with time, we let ϵ be governed by a first-order Butterworth filter as

$$\nu\epsilon' + \epsilon = \eta + \frac{1}{\eta} \tag{48}$$

where ν is a nondimensional time constant and

$$\eta = \epsilon\left[1-\alpha\Psi\right] \tag{49}$$

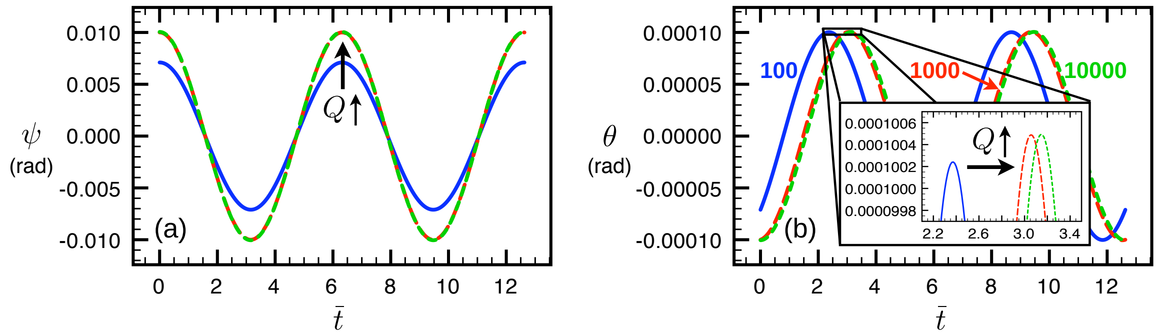

Figure 5. LIMIT CYCLES FOR (a) ψ AND (b) θ FOR THE FILTERED SYSTEM (EQNS. (26)) WITH $Q = 100, 1000$, OR 10000 AND ϵ SATISFYING EQN. (45) WITH $\epsilon = 2$, 10.1, OR 100.01, RESPECTIVELY. THE OTHER PARAMETERS USED ARE $\beta = 10$, $\lambda = 1$, $\zeta_{\mathrm{a}} = \zeta_{\mathrm{s}}$, $\alpha = 20000$, $\omega_{\mathrm{f}} = 0.00001$, AND $\zeta_{\mathrm{f}} = 1$.

is the nondimensional adaptive feedback gain. The gain adapts with the motion through a filter for stability purposes, and a first-order Butterworth filter was chosen because it is easily implemented in an analog circuit. Furthermore, we note that the adaptive feedback gain η depends on Ψ and therefore the oscillator motion.

Thus, the system that achieves a sinusoidal limit cycle for θ (Goal 2) with $A_\psi \gg A_\theta$ (Goal 1) and $A_\theta \not\approx f(Q)$ (Goal 3) is

$$\psi'' + 2\zeta\psi' + \psi + \theta = 0 \tag{50a}$$

$$\lambda\theta'' + 2\zeta\lambda\beta\theta' + (1 + \lambda\beta^2)\theta + \psi = -\eta\psi' \tag{50b}$$

$$\Psi'' + 2\zeta_{\mathrm{f}}\omega_{\mathrm{f}}\Psi' + \omega_{\mathrm{f}}^2\Psi = \omega_{\mathrm{f}}^2(\psi')^2 \tag{50c}$$

$$\eta = \epsilon\,(1 - \alpha\Psi) \tag{50d}$$

$$\nu\epsilon' + \epsilon = \eta + \frac{1}{\eta} \tag{50e}$$

For example, Figure 6 shows the system responses for two different cases in which Q jumps from 1000 to 100 at approximately the 2000th cycle. Before the rapid decrease in Q, the amplitudes and gains in both cases approach steady values. However, after the change in Q, the gain ϵ adjusts to maintain $A_\theta \approx 0.0001$ for the limit cycle, while ψ is allowed to have a new limit cycle with a smaller amplitude because of the increased damping. Furthermore, we note that the two nondimensional system responses are very similar because $\lambda\beta^2 = 100$ for the "stiff" case in Fig. 6(a) and $\lambda = 100$ for the "heavy" case in Fig. 6(b).

To understand how well the controlled system works, the nondimensional limit-cycle amplitude A_θ is plotted in Fig. 7 as a function of the quality factor. As Q decreases from 1000 to 100 for the two systems of Fig. 6, Fig. 7(a) reveals that A_θ changes by only about 0.25 %. In fact, A_θ can "jump" at most by about 0.4 %, and that maximum shift drops to about 0.1 % as the systems quadruple in "stiffness" ($\lambda\beta^2$) or "heaviness" (λ) for the systems of Fig. 7(b).

These results show that the oscillator could be calibrated as a velocity standard in air and used in ultra-high vacuum for a velocity shift within 0.4 %. This is because the nondimensional frequency $\bar{\omega}$ changes insignificantly with Q, while the amplitude A_θ changes only slightly with Q, as seen in Fig. 7, resulting in a maximum velocity $\bar{\omega}A_\theta$ that changes only slightly with Q.

POTENTIAL AS AN AFM SENSOR

In FM-AFM [15], the AFM cantilever is kept oscillating with a fixed amplitude and constant frequency above a sample sample while being moved across the surface without tip-surface contact [16]. The resolution of the resulting surface image depends on the sensitivity of the cantilever frequency to stiffness changes. For a typical AFM cantilever, the relative frequency sensitivity is

$$\frac{\frac{\partial\omega}{\partial k}}{\omega} = \frac{1}{2k} \tag{51}$$

where ω is the first natural frequency and k is the cantilever stiffness. Consequently, for a frequency resolution of 0.05 Hz, a stiffness change of $\Delta k \approx 0.01$ N/m can be detected for a quartz tuning fork sensor with a stiffness of $k = 1800$ N/m and a frequency of $\omega = 2\pi(17$ kHz$)$. In this way, even sub-atomic (orbital) resolution imaging has been achieved [17].

Perhaps the micro-oscillator could be used in place of a quartz tuning fork as the sensor in FM-AFM, because the oscillation amplitude is controlled. However, a stiffness change at point P in Fig. 1(a) does not cause a significant change in the system frequency; the sensitivity is significantly lower than that in Eqn. (51). In contrast, the adaptive feedback gain η could be measured instead of the system frequency to track stiffness changes. During the limit-cycle oscillation, the adaptive feedback gain is constant and defined by Eqns. (44) and (49). Accordingly,

$$\frac{\frac{\partial\eta}{\partial k_{\mathrm{P}}}}{\eta} \approx \begin{cases} \frac{1}{k_{\mathrm{P}}} & \text{"stiff" case} \\ 0\,, & \text{"heavy" case} \end{cases} \tag{52}$$

where k_{P} is the stiffness of point P in Fig. 1(a). With a feedback voltage of 1 V and a voltage resolution of 0.1 μV, a stiffness

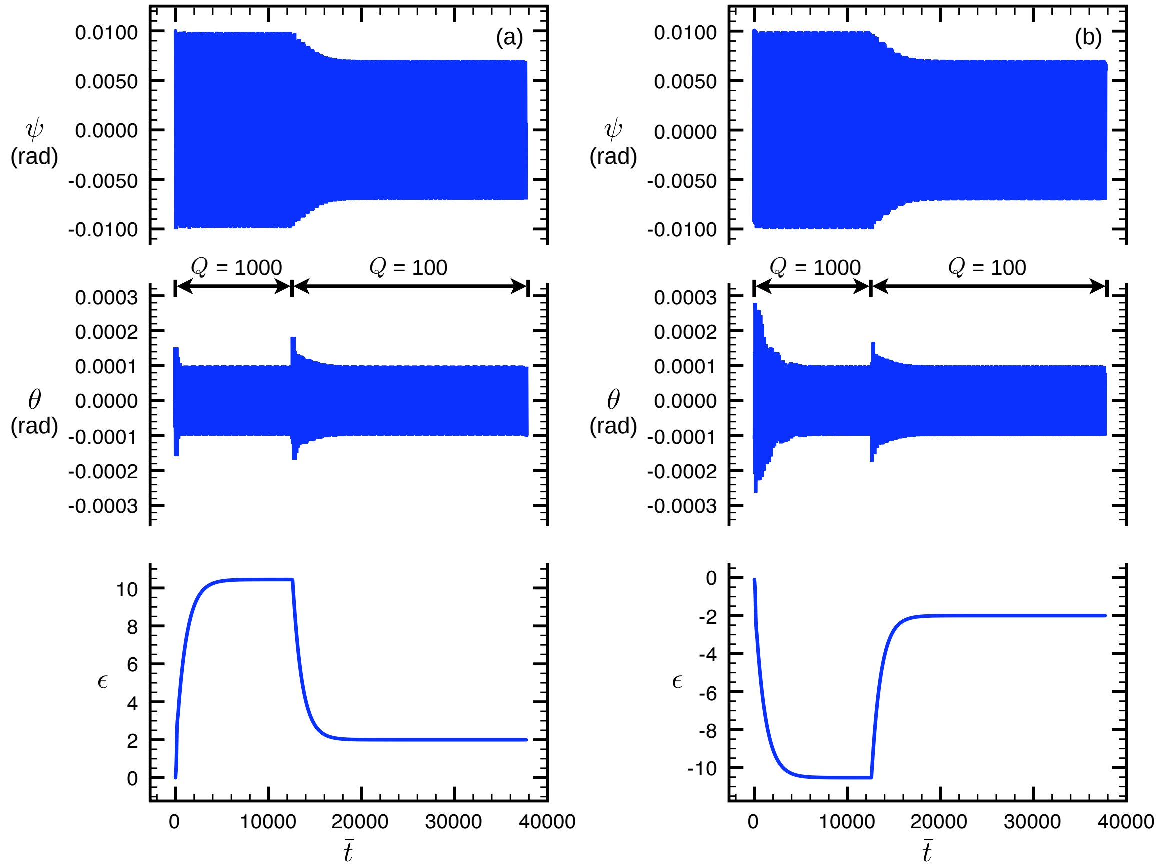

Figure 6. RESPONSE OF THE CONTROLLED SYSTEM (EQNS. (50)) VERSUS NONDIMENSIONAL TIME $\bar{t}$ WITH (a) $\beta = 10$ AND $\lambda = 1$ (A "STIFF" CASE) OR (b) $\beta = 0.1$ AND $\lambda = 100$ (A "HEAVY" CASE). THE QUALITY FACTOR Q JUMPS FROM 1000 TO 100 AT $\bar{t} = 2000(2\pi)$. THE OTHER PARAMETERS USED ARE $\zeta_{\mathrm{a}} = \zeta_{\mathrm{s}}$, $\alpha = 20000$, $\omega_{\mathrm{f}} = 0.05$, $\zeta_{\mathrm{f}} = 1$, AND $\nu = 1000$. THE THREE PLOTS WITHIN A SUBFIGURE HAVE THE SAME ABSCISSA SEEN AT THE BOTTOM OF THE SUBFIGURE.

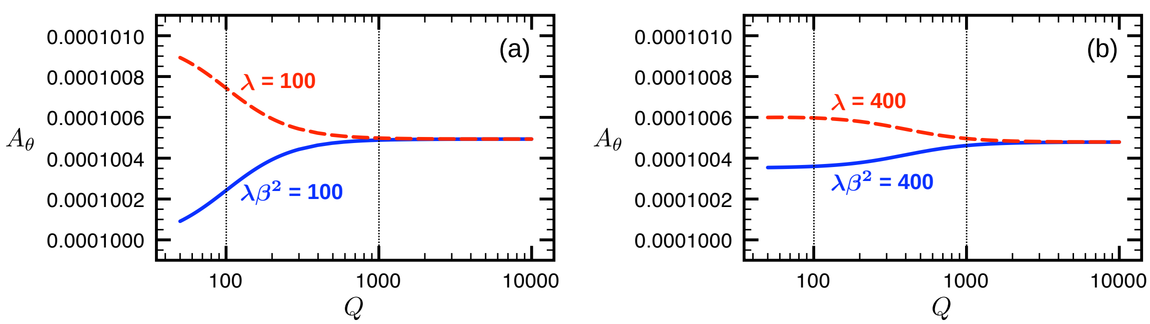

Figure 7. THE NONDIMENSIONAL LIMIT-CYCLE AMPLITUDE A_θ AS A FUNCTION OF THE QUALITY FACTOR Q FOR THE CONTROLLED SYSTEM (EQNS. (50)) WITH (a) $\beta = 10$ AND $\lambda = 1$ (SOLID CURVE) OR $\beta = 0.1$ AND $\lambda = 100$ (DASHED CURVE), OR (b) $\beta = 10$ AND $\lambda = 4$ (SOLID CURVE) OR $\beta = 0.1$ AND $\lambda = 400$ (DASHED CURVE). THE PARAMETER α WAS SET TO EITHER (a) 20000 OR (b) 12600 WITH $\zeta_{\mathrm{a}} = \zeta_{\mathrm{s}}$ AND THE 2ND-ORDER FILTER BEING "PERFECT" ($\omega_{\mathrm{f}} \approx 0$).

change of $\Delta k_{\mathrm{P}} = 0.01$ N/m can be detected for the "stiff" case with an actuation stiffness of k_{P} = 100 kN/m. Consequently, the smallest detectable stiffness change is potentially on the order of that for present FM-AFM methods used to achieve atomic resolution. Furthermore, one micro-oscillator could be used to calibrate another in order to determine the stiffness k_{P} and hence the sensitivity defined by Eqn. (52).

CONCLUSIONS

A new self-excited micro-oscillator based on magnetic sensing and actuation was developed as a velocity standard for use in the measurement of SI-traceable nanonewton-level forces. An analog control scheme was devised to yield an oscillation amplitude that is fairly insensitive to the quality factor. Consequently, it was shown that the micro-oscillator could be calibrated as a velocity standard in air and then used in ultra-high vacuum with a velocity shift within about $0.4\ \%$. The micro-oscillator may then be used to calibrate AFM cantilevers by means of SI-traceable electrostatic nanonewton-level forces according to standards of the National Institute of Standards and Technology (NIST). Furthermore, the calibrated micro-oscillator could potentially be used as an AFM sensor to achieve atomic resolutions on par with those realized with quartz tuning forks in FM-AFM.

ACKNOWLEDGMENTS

Thanks go to Jason Gorman, Gordon Shaw, and John Kramar (Manufacturing Engineering Laboratory) as well as Alex Liddle and Jason Crain (Center for Nanoscale Science and Technology) at NIST for their constructive advice towards this work. Many thanks also go to NIST and the National Research Council (NRC) for sponsoring Gregory W. Vogl as a postdoctoral research associate.

REFERENCES

[1] Binnig, G., Quate, C. F., and Gerber, Ch., 1986. "Atomic force microscope". *Physical Review Letters,* **56**(9), pp. 930–933.

[2] Giessibl, F. J., 1995. "Atomic resolution of the silicon (111)-(7×7) surface by atomic force microscopy". *Science,* **New Series, 267**(5194), pp. 68–71.

[3] Kitamura, S., and Iwatsuki, M., 1995. "Observation of 7×7 reconstructed structure on the silicon (111) surface using ultrahigh vacuum noncontact atomic force microscopy". *Japanese Journal of Applied Physics,* **34**(2(1B)), pp. L145–L148.

[4] Cross, B., Ronzon, F., Roux, B., and Rieu, J.-P., 2005. "Measurement of the anchorage force between GPI-anchored alkaline phosphatase and supported membranes by AFM force spectroscopy". *Langmuir,* **21**, pp. 5149–5153.

[5] Sonnenberg, L., Parvole, J., Borisov, O., Billon, L., Gaub, H. E., and Seitz, M., 2006. "AFM-based single molecule force spectroscopy of end-grafted poly(acrylic acid) monolayers". *Macromolecules,* **39**, pp. 281–288.

[6] Hutter, J. L., and Bechhoefer, J., 1993. "Calibration of atomic-force microscope tips". *Review of Scientific Instruments,* **64**(7), pp. 1868–1873.

[7] Butt, H.-J., and Jaschke, M., 1995. "Calculation of thermal noise in atomic force microscopy". *Nanotechnology,* **6**(1), pp. 1–7.

[8] Cleveland, J. P., Manne, S., Bocek, D., and Hansma, P. K., 1993. "A nondestructive method for determining the spring constant of cantilevers for scanning force microscopy". *Review of Scientific Instruments,* **64**(2), pp. 403–405.

[9] Sader, J. E., Larson, I., Mulvaney, P., and White, L. R., 1995. "Method for the calibration of atomic force microscope cantilevers". *Review of Scientific Instruments,* **66**, pp. 3789–3798.

[10] Koch, S. J., Thayer, G. E., Corwin, A. D., and de Boer, M. P., 2006. "Micromachined piconewton force sensor for biophysics investigations". *Applied Physics Letters,* **89**, pp. 173901–1–173901–3.

[11] Gates, R. S., and Pratt, J. R., 2006. "Prototype cantilevers for SI-traceable nanonewton force calibration". *Measurement Science and Technology,* **17**, pp. 2852–2860.

[12] Vogl, G. W., Gorman, J. J., Shaw, G. A., and Pratt, J. R., 2008. "A new microdevice for SI-traceable forces in atomic force microscopy". In Proceedings of the SEM XI International Congress & Exposition on Experimental and Applied Mechanics.

[13] Cumpson, P. J., and Hedley, J., 2003. "Accurate analytical measurements in the atomic force microscope: a microfabricated spring constant standard potentially traceable to the SI". *Nanotechnology,* **14**, pp. 1279–1288.

[14] Nayfeh, A. H., 1981. *Introduction to Perturbation Techniques*. John Wiley & Sons, Inc., New York, p. 147.

[15] Albrecht, T. R., Grütter, P., Horne, D., and Rugar, D., 1991. "Frequency modulation detection using high-Q cantilevers for enhanced force microscope sensitivity". *Journal of Applied Physics,* **69**(2), pp. 668–673.

[16] Giessibl, F. J., and Bielefeldt, H., 2000. "Physical interpretation of frequency-modulation atomic force microscopy". *Physical Review B,* **61**(15), pp. 9968–9971.

[17] Giessibl, F. J., Hembacher, S., Bielefeldt, H., and Mannhart, J., 2000. "Subatomic features on the silicon (111)-(7×7) surface observed by atomic force microscopy". *Science,* **289**(5478), pp. 422–425.